

Characteristic Airflow Patterns During Inspiration and Expiration: Experimental and Numerical Investigation

Mohammed Zubair¹ · Kamarul Arifin Ahmad¹ · Mohd. Zulkifty Abdullah² · Shaker Farid Sufian²

Received: 9 February 2014 / Accepted: 3 June 2014 / Published online: 3 June 2015
© Taiwanese Society of Biomedical Engineering 2015

Abstract A simplified experimental nasal model was designed and an experimental setup was developed to facilitate both inspiratory and expiratory flow measurements. Particle image velocimetry (PIV) and resistance measurements were conducted. The purpose of this work was primarily to demonstrate a simple way of carrying out experiments for a replica human nose in order to validate numerical studies. The characteristic recirculatory patterns observed explicitly as a consequence of inspiration and expiration were investigated. The resistance study showed similar patterns of resistance for both experimental and numerical results for various flow rates. The PIV results showed that inspiratory and expiratory flows had characteristic flow patterns that can be distinguished based on their recirculatory flow patterns.

Keywords Computational fluid dynamics (CFD) · Particle image velocimetry (PIV) · Nasal cavity · Inspiration · Expiration

1 Introduction

The primary functions of human airways are transporting oxygen to the lungs and removing carbon dioxide. The human nasal cavity is ideally suited to perform

physiological functions such as maintaining an appropriate air flow. However, the understanding of its physiological functions is limited to that obtained via clinical inferences or objective measurement devices such as rhinomanometry. These devices have limited scope and fail to provide detailed flow physics inside the complicated nasal architecture.

A recent advance in biomedical engineering is the application of numerical methods for understanding flow characteristics associated with the nose. In recent years, usage of computational fluid dynamics (CFD)-based software tools has revolutionized the biomedical field and has enhanced our understanding of vital human anatomical functions [1–3]. Computed tomography (CT) scans or magnetic resonance images coupled with CFD tools are extensively used for determining the nasal resistance at any desired location. Recent studies using CFD have provided a wealth of information on nasal physiology. However, most CFD modeling of nasal airflow is based on the inspiratory breathing mechanism. Zubair et al. [4] and Wen et al. [5] discussed the formation of recirculatory flow patterns near the olfactory cells during inspiration. Keyhani et al. [3] determined that approximately 10 % of inspired air passes through the olfactory cleft. Moreover, the percentage of flow decreases towards the posterior end of the olfactory cleft as a result of the steep downward bend in the nasal roof. In most of these studies, the discourse was limited to inspiratory flow, with the effect of expiratory phenomenon on olfactory region not discussed. Therefore, additional studies are necessary to ascertain the specific physiological differences between inspiration and expiration.

Validation of CFD studies is another important concern. Previous researchers have utilized several methods to fabricate in vitro nasal cavity models. Spence et al. [6] studied nasal airflow using particle image velocimetry (PIV). Hahn

✉ Mohammed Zubair
mdzubairmanipal@gmail.com

¹ Department of Aerospace Engineering, Universiti Putra Malaysia, 43400 Serdang, Selangor, Malaysia

² School of Mechanical Engineering, Universiti Sains Malaysia, Engineering Campus, 14300 Nibong Tebal, Malaysia

et al. [7] created a scale model by glueing 169 styrofoam slabs (40 mm thick) together. Similarly Doorly et al. [8] used a 2×-scale model created on a three-dimensional (3D) printer [8]. This porous prototype was sealed using fine layers of polyvinyl acetate, and then placed inside an acrylic box mould, which was filled with a silicone elastomer of optically transparent grade. When the silicone was cured, the acrylic box was removed and the model was immersed in water to dissolve the prototype and its coating, which yielded a transparent silicone block encasing the replica nasal airway geometry. There are several disadvantages to using this design. The main ones are the inclusion of unnecessary steps and time-consuming manufacturing. In addition, the casting of silicone on a nasal model requires a lot of precision. It can lead to distortion of the actual geometry as well as shrinkage. Moreover, a cast model does not allow the cleaning of internal surfaces. A nasal model is a complicated structure, and any attempt to insert cleaning agents may harm the optical surface.

In the present study, a simplified experimental nasal model is designed and an experimental setup is developed to facilitate both inspiratory and expiratory flow measurements. Results obtained from PIV studies are compared with those from CFD simulations. The CFD simulations are carried out using water as the fluid medium. This work is an extension of the work carried out by Riazuddin et al. [2].

2 Method

2.1 Experimental Investigations

In order to develop a 3D experimental model, *.iges file obtained from MIMICS were utilized and exported to CATIA workbench. The process of developing a 3D nasal cavity model from CT images is shown in Fig. 1. The developed 3D model can be used for both experimental and numerical studies. In the present work, the 2×-scale left half of the nasal cavity was developed and manufactured using a 3D rapid prototyping machine at SIRIM Berhad, Malaysia. Considering the difficulty in visualization and carrying out experiments with a full model, it was decided to use only one half of the nasal cavity. It was found that the left section of the nasal cavity had a larger cross-sectional area and was less complicated compared to the right half. Therefore, only the left half of the nasal cavity was developed in CATIA workbench. Unlike previous models, the current model utilized a material which produced a transparent model. This material, DSM Somos[®] 11120, is a low-viscosity liquid photopolymer that produces strong, tough, and water-resistant parts. This simplified the entire process and avoided the need to cast a silicone elastomer. In order to facilitate a hollow cavity model, a new design

was proposed, as shown in Fig. 2a and b. This design has two complimentary parts of the left cavity embedded in a rectangular tablet. The final printed left nasal cavity with a nostril and the nasopharynx is shown in Fig. 2c.

The PIV experimental rig is shown in Fig. 3. The PIV system consists of a pulsed diode laser, a Flow Sense 2 M 10-bit camera, a synchronizing timing hub, and a Dell Precision system. Flow Manager TM V4.6 software was used to obtain images and compute the velocity fields. The flow was illuminated using frequency doubling with a non-linear crystal as a second harmonic generator, which converts the infrared light to visible green light ($\lambda = 532$ nm) with a pulsed beam generated by a Nd:YAG laser with a power of 850 mJ/pulse. Images of the flow field were captured using a 1600 × 1186 pixel CCD camera with 10-bit intensity resolution. The second frame was recorded continuously, with 4 μs for each frame. A Nikkor 60 mm, F:2.8D standard lens was used with variable zoom to obtain image magnifications of lower than 3 μm/pixel. The camera was placed outside the enclosure, perpendicular to the laser sheet. The laser sheet was positioned to illuminate the flow field at the center of the tablet along the horizontal plane from the front side and the camera was positioned in the vertical plane to capture the flow field on the top surface of the tablet. The seeding material used was titanium dioxide (TiO₂), of micro size, which had demonstrated better properties with respect to laser light reflection when compared to glass beadings. This closed-loop experimental rig used water as the flow medium. In order to determine the resistance offered by the nasal cavity, flow rates ranging from 1 to 2.8 m³/h were applied. A rotameter attached to the pump was used to read the mass flow rate of water.

2.2 Numerical Investigations

2.2.1 Governing Equations

The steady-state continuity and momentum equations in Cartesian tensor notation can be expressed as:

$$\frac{\partial}{\partial x_i} (\rho_w u_i^w) = 0 \quad (1)$$

$$\rho_w u_j^w \frac{\partial u_i^w}{\partial x_j} = -\frac{\partial p_w}{\partial x_i} + \frac{\partial}{\partial x_j} \left(\mu_g \frac{\partial u_i^w}{\partial x_j} \right) \quad (2)$$

where u_i^w is the i th component of the time-averaged velocity vector, ρ_w is the water density, and μ_g is the viscosity.

The shear-stress transport (SST) k - ω model developed by Menter is used to effectively blend the robust and accurate formulation of the k - ω model in the near-wall region with the free-stream independence of the k - ϵ model in the far field [10].

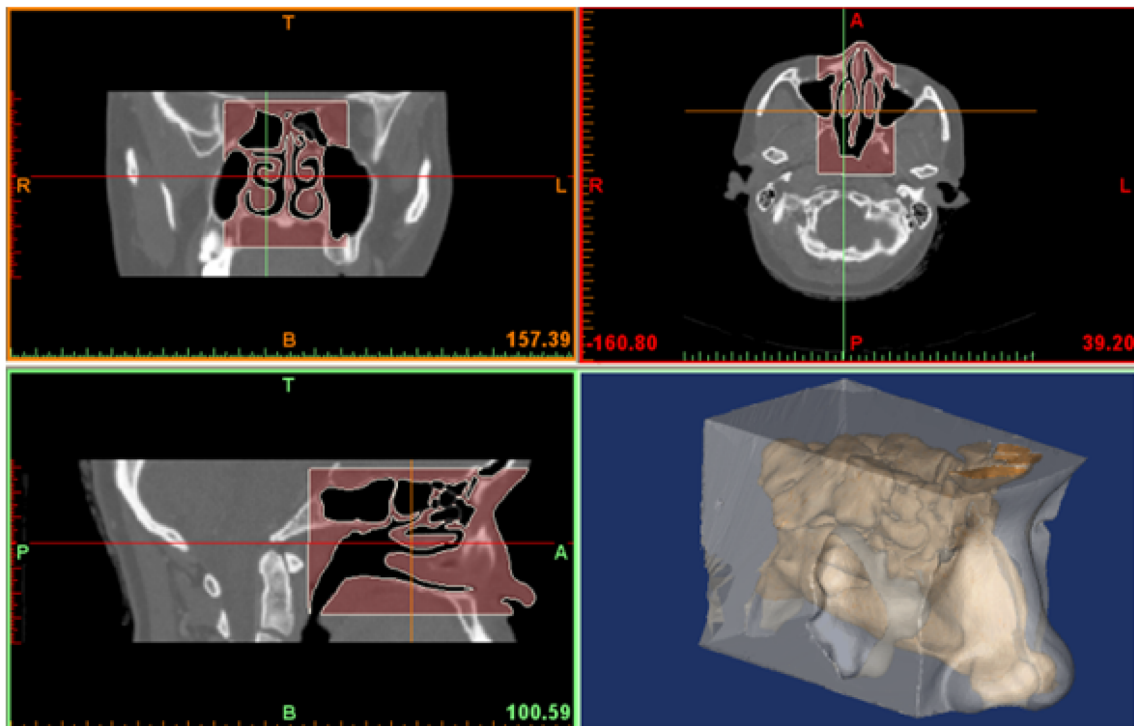
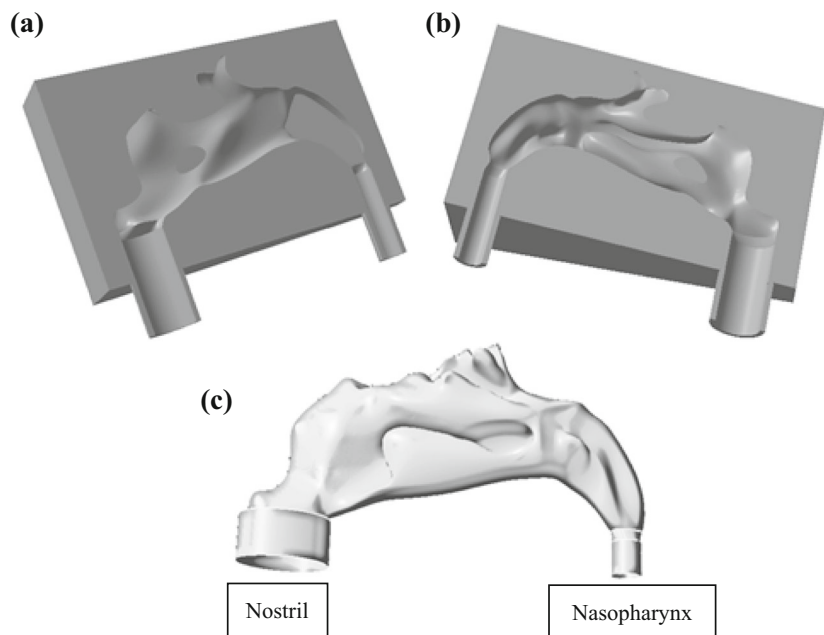


Fig. 1 CT scan images and 3D model of human nasal cavity

Fig. 2 **a** Left and **b** right halves of the left nasal cavity model and **c** full nose model with its salient features

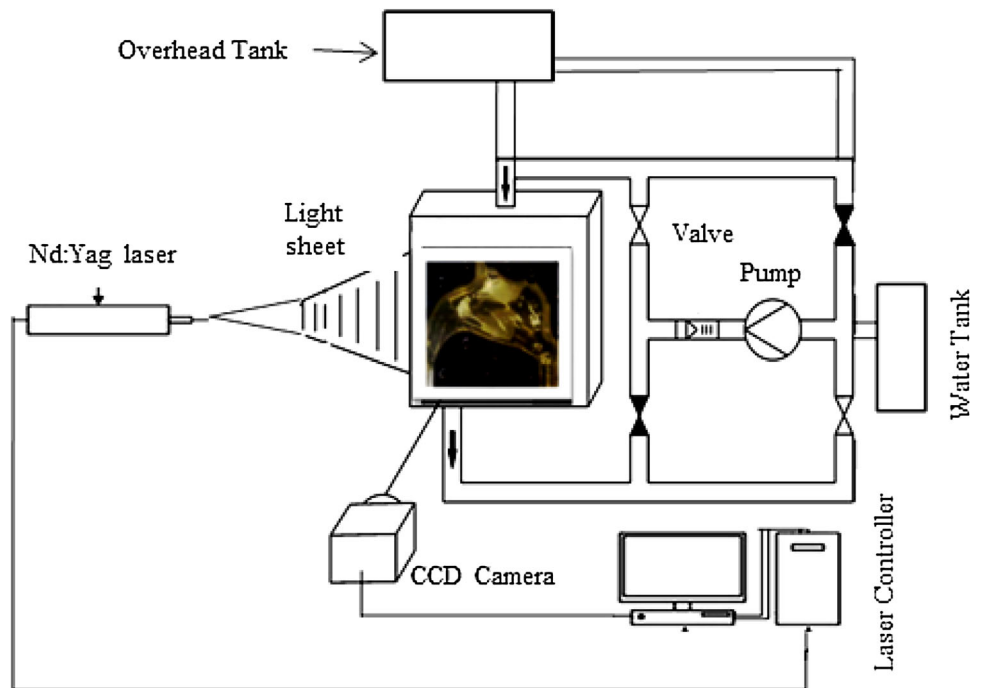


2.2.2 Numerical Modeling

The 3D polyline data of the nasal cavity were edited in CATIA and meshed with a hybrid mesh generated using Tgrid and GAMBIT (Fluent, Lebanon, NH). A 2x-scale model of the left half of the nasal cavity was meshed in GAMBIT, which resulted in a mesh count of 319,450

elements. The hybrid mesh consisted of a combination of 6 layers of prism cells near the near-wall boundary and tetrahedral elements in the remaining flow domain. The numerical simulation was carried out using the commercial CFD solver FLUENT 6.3. Water was used as the fluid medium and the simulation was carried out for flow rates of 1.2, 1.6, 2.0, 2.4, and 2.8 m³/h, similar to those used for

Fig. 3 Schematic diagram of PIV experimental setup



experimental investigations. The simulation solves the Reynolds-averaged Navier–Stokes equation, which is the general equation for the 3D flow of incompressible and viscous fluids. A two-equation SST turbulence $k-\omega$ model was employed [2, 9].

The nasal wall was assumed to be rigid and the simulation ignored the presence of mucus. A no-slip boundary condition was defined at the walls. A plug flow boundary condition was implemented for the inspiration case, with the mass flow rate imposed at the nostril inlet and the outflow boundary defined at the nasopharynx outlet (Fig. 4). The velocity or pressure at the nasopharynx is not known prior to the solution of the flow problem. This is because the nasopharynx continues to the oro-pharynx section and then to the lungs via the bronchi. Therefore, the outflow boundary condition was utilized to model the nasopharynx exit during inspiration. The outflow boundary conditions in FLUENT are used to model flow exits where the details of the flow velocity and pressure are not known prior to the solution of the flow problem. FLUENT extrapolates the required information from the interior. For the exhalation phenomenon pressure outlet was defined at the nostril and the mass flow rate at the nasopharynx.

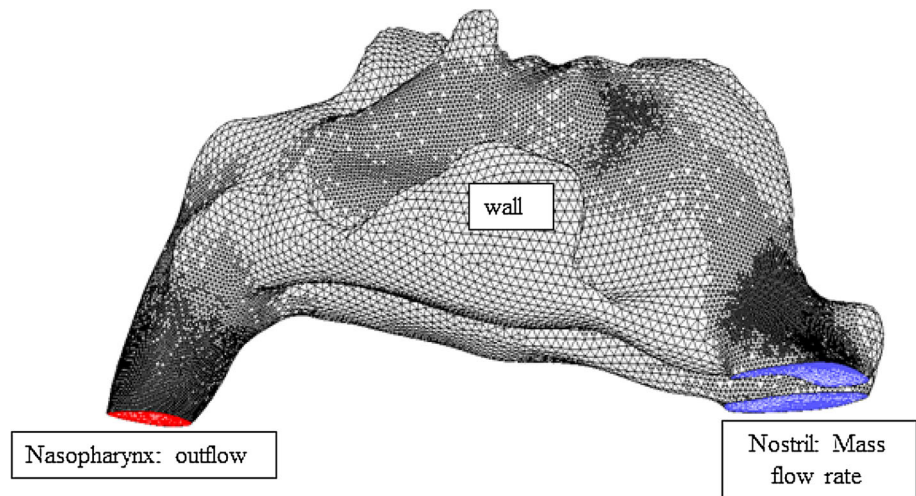
3 Results and Discussion

The primary objective of this work was to establish a simple way of conducting experiments inside the complicated nasal cavity. Previous works used a casting method to develop 3D nasal models for carrying out PIV studies [6–8]. In general, this involves two main steps. In the first step,

the 3D solid model is developed using a water soluble material. In the second step, this water soluble material is cast in an acrylic box into which the molten silicone is poured and cured. The resultant model is immersed in water for several hours to dissolve the solid nasal model, leaving behind a clear hollow cavity inside the transparent acrylic box. This procedure is very expensive as it involves several steps. Moreover, the time required to develop the final model is very high and the process involves unnecessary steps that can be easily avoided. In addition, the accuracy of the developed model can be affected by factors such as shrinkage and temperature. In PIV studies, there is a tendency for seeding particles to attach to the nasal wall, which may harm the optical surface and thus reduce visibility. During experiments, there is a high possibility of blockage or pigmentation owing to the deposition of seeding particles. This pigmentation must be removed to allow further experimentation. The present model was manufactured in two coupling parts that can be easily disassembled after every experiment and cleaned for reuse (Fig. 2). This ensures maximum optical visualization and limits false vectors due to distortion of laser reflection by previously deposited particles. Experiments were carried out for flow rates of 1.2, 1.6, 2.0, 2.4, and 2.8 m³/h. The model was cleaned before every experiment to remove the deposited nanoparticles used as the seeding material. [Researchers can now benefit from this simple 3D nasal model by writing to the authors for more information].

In this section, two validation methods are described and their results are compared with the outcome of the numerical investigation. The first method is the calculation of

Fig. 4 Volume mesh of 3D computational model of human nasal cavity



resistance offered by the nasal cavity based on the works of Wen et al. [4] and Zubair et al. [5]. In order to determine the resistance offered by the nasal cavity, the experimental model was subjected to flow rates ranging from 1 to 2.8 m³/h. Figure 5 compares the experimental and numerical values of resistance at various flow rates. It clearly shows that the resistance obtained from the numerical simulation closely matches that of the experiment. The resistance offered by the nasal cavity for a flow rate of 2.0 m³/h was estimated to be about 735.1 and 735.6 Pa min/L for experimental and numerical models, respectively. This shows that the numerical model used in this study agrees well with the experimental results.

The other method used for validation was PIV. The regions of recirculatory flow observed at two locations that distinguish inspiratory and expiratory flow were considered as the benchmark for carrying out the PIV experimental validation. This is because the two regions have unique features that clearly distinguish the inspiratory and

expiratory flow and provide clear evidence of the flow physics inside the nasal cavity. The two locations identified are the posterior region just before the nasopharynx bend and the anterior region near the roof of the nose. This was in accordance with our previous study on inspiratory and expiratory flow analysis [2]. Inspiration and expiration offer different insights into flow owing to their different flow directions.

Figure 6 shows a snapshot of the anterior portion of the nasal cavity near the roof of the nasal cavity. Olfactory cells, responsible for the sense of smell, are located in this region. It can be seen from both the numerical and experimental findings that during inspiration, a recirculatory flow forms near the olfactory cells. Similar findings have been reported by many researchers, who observed that the flow entering the olfactory region is recirculatory flow [3–5]. The significance of the olfactory region stems from the fact that it houses the olfactory nerves whose function is to distinguish different smell perceptions. Thus, in order to stimulate the olfactory system (sense of smell), the odorant particles must interact with olfactory receptors located in the olfactory mucosa. In order to facilitate this, the odorants must be capable of being delivered to the olfactory region by inspired air and be able to dissolve sufficiently in the mucus covering the olfactory mucosa [11]. The human nasal anatomy is designed to facilitate this action, which is accomplished via recirculation of air in the olfactory vicinity. The advantage of this low-velocity recirculatory flow is that it allows odorant particles to reside in the region for a longer duration and therefore helps smell identification and analysis. Therefore, any abnormality in the olfactory region can seriously affect the recirculatory behavior and hamper the ability to smell. This was confirmed by Zhao et al. [12], who carried out numerical simulations and showed that a small (1.45 %) reduction of the local airway volume can result in an 18.7 % decrease in the

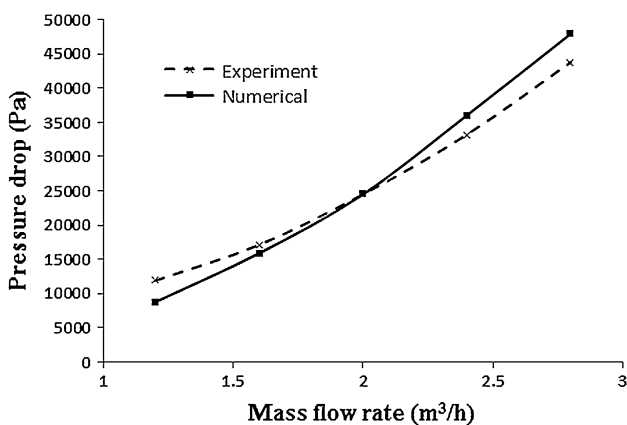


Fig. 5 Nasal resistance obtained from experimental and numerical studies

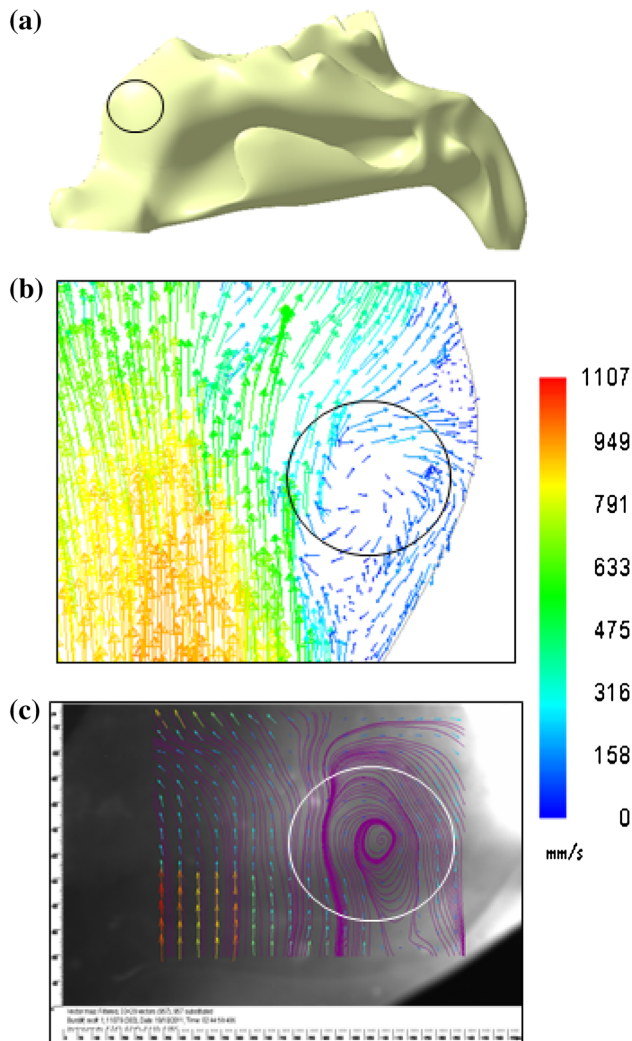


Fig. 6 Comparison of inspiratory flow in *anterior region*. **a** Nasal model highlighting *anterior location*, **b** numerical results, and **c** PIV experiment results

global air flow rate through the nostril and a 76.9 % decrease in the local olfactory air flow rate. The interesting feature of this location in the anterior portion is that this recirculatory behavior is typical of only inspiration. The expiratory flow does not demonstrate any recirculatory behavior. The vectors shown in Fig. 7a and b are directed out, indicating that the flow motion is towards the nostril exit. The non-occurrence of any recirculatory pattern during expiration explains the inability to smell during exhalation. Thus, it can be concluded that, it is impossible for humans to detect any smell during expiration.

Some interesting findings were observed at the posterior location of the nasal cavity. It can be clearly seen in Fig. 8a and b that during inhalation, the vectors are directed towards the exit of the nasopharyngeal section. The mean velocity in this section is about 0.2–0.4 m/s. No divergence of vectors is observed during inhalation. In contrast,

expiratory flow demonstrated recirculatory behavior, as shown in Fig. 9a and b. It can therefore be concluded that the expiratory flow exhibits recirculation of air near the posterior region just beyond the nasopharynx. The combination of the nasopharyngeal bend and the inferior turbinates accounts for this recirculatory behavior during expiration. The flow entering into the nasal cavity is thrown upwards due to the nasopharyngeal bend while the floor receives much less flow. This low-velocity flow is further obstructed by the lips of the inferior turbinates, causing the flow to circulate in that region. The expiratory flow carries with it moisture and heat, which is absorbed by the turbinates. This recirculatory behavior facilitates the exchange of heat and moisture with the surrounding turbinates. This recirculatory behavior transfers the heat and humidity from the outgoing airflow back to the middle turbinates and therefore acts as an efficient energy saving

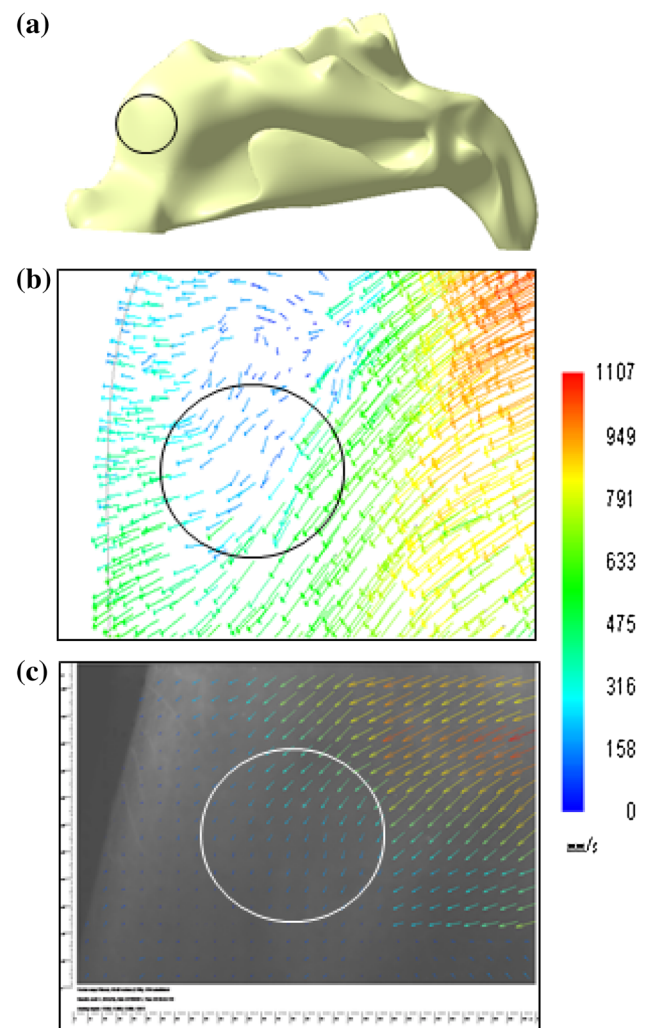


Fig. 7 Comparison of expiratory flow in *anterior region*. **a** Nasal model highlighting *anterior location*, **b** numerical results, and **c** PIV experiment results

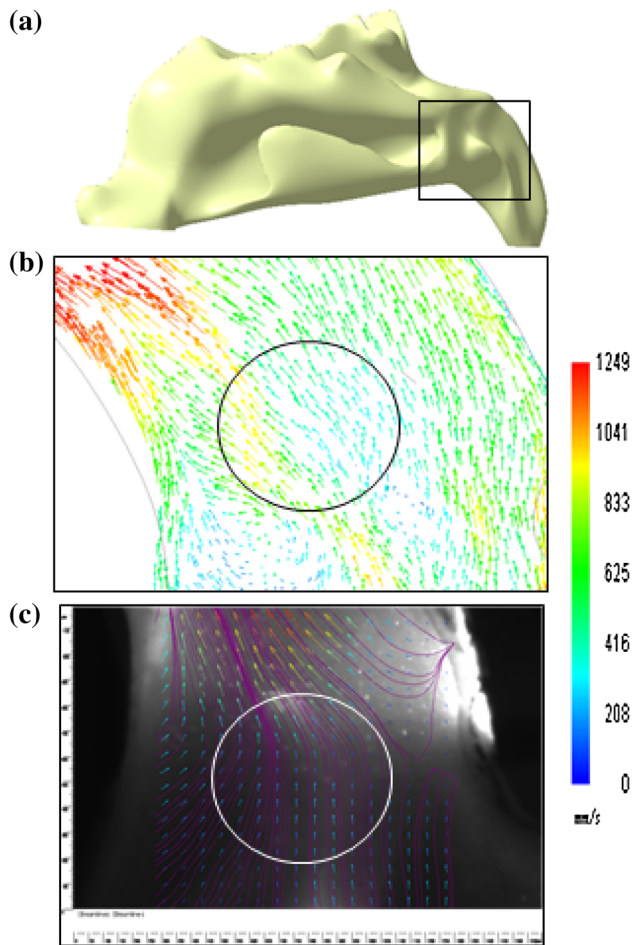


Fig. 8 Comparison of inspiratory flow in *posterior end*. **a** Nasal model highlighting *posterior location*, **b** numerical results, and **c** PIV experiment results

system [13–14]. The vortex formation during expiration results in the efficient mixing of air, and vapor from the mucous secretion also helps the exchange of heat from the blood vessels situated in the area.

This was only typical of expiratory flow. No such recirculation was observed during inspiration, as shown in Fig. 8a and b. This phenomenon was corroborated by CFD studies for several other nasal cavity models (results not shown). Thus, the inspiratory and expiratory flows can be distinguished by their characteristic recirculatory flows in the anterior and posterior regions, respectively. Thus, it can be concluded that the experimental findings well match the results of the numerical study.

4 Conclusion

An easy design for carrying out PIV experiments was demonstrated in this study. Recirculatory regions that differentiate inspiratory flow from expiratory flow were

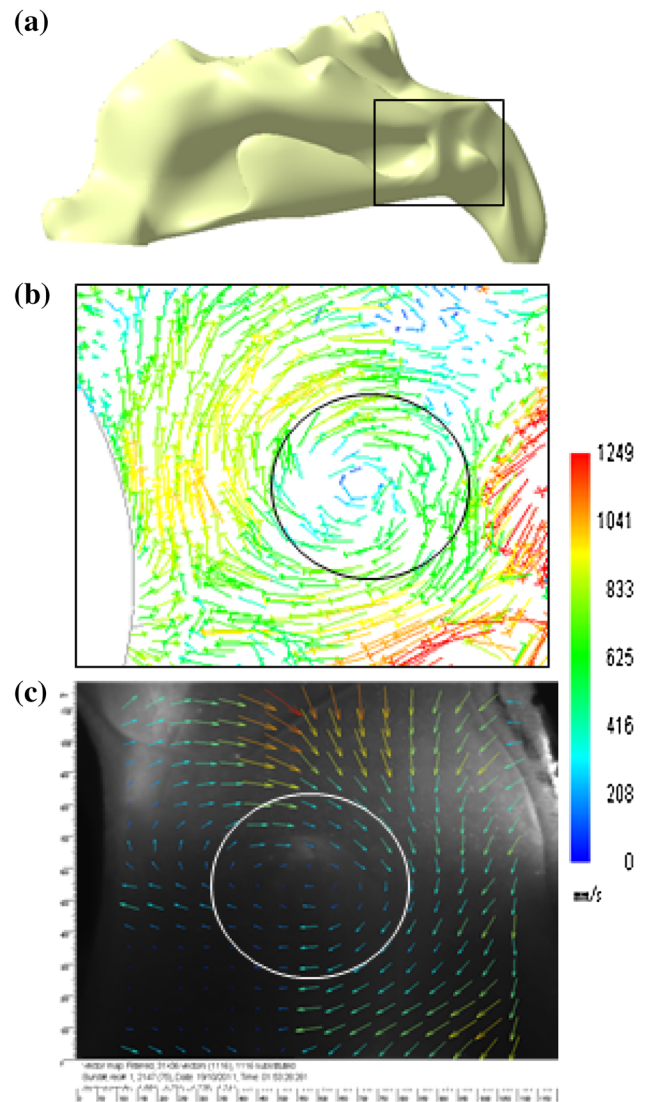


Fig. 9 Comparison of expiratory flow in *posterior end*. **a** Nasal model highlighting *posterior location*, **b** numerical results, and **c** PIV experiment results

identified for use as the benchmark for experimental validation studies. The resistance offered by the nasal cavity for a flow rate of 2.0 m³/h was estimated to be about 735.1 and 735.6 Pa min/L for experimental and numerical models, respectively. This shows that the numerical model agrees well with the experimental results. During inspiration, recirculatory flow behavior was observed in the anterior region near to the olfactory cells, which helps the sense of smell. During expiration, recirculatory flow was observed close to the beginning of the nasopharyngeal section, which helps moisture and heat exchange.

Acknowledgments The authors acknowledge the support of the Geran Universiti Putra Malaysia and Fundamental Research Grant Scheme (FRGS).

References

1. Zubair, M., Abdullah, M. Z., & Ahmad, K. A. (2013). Hybrid mesh for nasal airflow studies. *Computational and Mathematical Methods in Medicine*, 1–7, 2013.
2. Riazuddin, V. N., Zubair, M., Abdullah, M. Z., Ismail, R., Shuaib, I. L., Suzina, A. H., & Ahmad, K. A. (2011). Numerical study of inspiratory and expiratory flow in a human nasal cavity. *Journal of Medical and Biological Engineering*, 31, 201–206.
3. Keyhani, K., Scherer, P. W., & Mozell, M. M. (1995). Numerical simulation of airflow in the human nasal cavity. *Journal of Biomechanical Engineering*, 117, 429–441.
4. Zubair, M., Riazuddin, V. N., Abdullah, M. Z., Ismail, R., Shuaib, I. L., Suzina, A. H., & Ahmad, K. A. (2013). Computational fluid dynamics study of the effect of posture on airflow characteristics inside the nasal cavity. *Asian Biomed*, 7, 835–840.
5. Wen, J., Inthavong, K., Tu, J., & Wang, S. (2008). Numerical simulations for detailed airflow dynamics in a human nasal cavity. *Respiratory Physiology & Neurobiology*, 161, 125–135.
6. Spence, C. J. T., Buchmann, N. A., Jermy, M. C., & Moore, S. M. (2011). Stereoscopic PIV measurements of flow in the nasal cavity with high flow therapy. *Experiments in Fluids*, 50, 1005–1017.
7. Hahn, I., Scherer, P. W., & Mozell, M. M. (1993). Velocity profiles measured for airflow through a large-scale model of the human nasal cavity. *Journal of Applied Physiology*, 75, 2273–2287.
8. Doorly, D., Taylor, D. J., Franke, P., & Schroter, R. C. (2008). Experimental investigation of nasal airflow. *Part H: Journal of Engineering in Medicine*, 222, 439–453.
9. Zubair, M., Abdullah, M. Z., Ismail, R., Shuaib, I. L., Suzina, A. H., & Ahmad, K. A. (2012). Review: Critical overview of limitations of CFD modeling of nasal airflow. *Journal of Medical and Biological Engineering*, 32, 77–84.
10. Menter, F. R. (1994). Two-equation eddy-viscosity turbulence models for engineering applications. *AIAA journal*, 32, 1598–1605.
11. Ishikawa, S., Nakayama, T., Watanabe, M., & Matsuzawa, T. (2006). Visualization of flow resistance in physiological nasal respiration: analysis of velocity and vorticities using numerical simulation. *Archives of Otolaryngology: Head & Neck Surgery*, 132, 1203–1209.
12. Zhao, K., Scherer, P. W., Hajiloo, S. A., & Dalton, P. (2004). Effect of anatomy on human nasal airflow and odorant transport patterns: implications for olfaction. *Chemical Senses*, 29, 365–379.
13. Zubair, M., Riazuddin, V. N., Abdullah, M. Z., Rushdan, I., Shuaib, I. L., & Ahmad, K. A. (2013). Computational fluid dynamics study of pull and plug flow boundary condition on nasal airflow. *Biomedical Engineering: Applications, Basis and Communications*, 25, 1350044–1350051.
14. Zhu, J. H., Lim, K. M., Gordon, B. R., Wang, D. Y., & Lee, H. P. (2014). Effects of anterior ethmoidectomy with and without antrotomy and uncinectomy on nasal and maxillary sinus airflows: a CFD study. *Journal of Medical and Biological Engineering*, 34, 144–149.